# EXPERIMENTAL AND NUMERICAL EVALUATION OF LNAPL LENS AND POLLUTED CAPILLARY FRINGE THICKNESS



By Lizette R. Chevalier,[1] Member, ASCE

**ABSTRACT:** The effective remediation of light non-aqueous-phase liquid (LNAPL) in the subsurface is dependent on predicting the location and geometry of the lens near the tension-saturated pores of the capillary fringe. The objective of this study was to evaluate both the thickness of a lens of light nonaqueous phase liquid spill in the subsurface and the subsequent alteration of the capillary fringe. Two-dimensional (2D) experiments were conducted in a parallel plate glass tank (1 m × 1 m × 5 cm) using Ottawa sand and gasoline. An equation for predicting the vertical thickness based on the displacement pressure in the lateral direction was developed. The model and previously published vertical equilibrium models for predicting the thickness of a lens were tested. The model equations were also used to evaluate changes in the capillary fringe due to capillary pollution. The results provide a means to better understand the behavior of light nonaqueous phase liquids in the subsurface.

## INTRODUCTION

Ground-water contamination from a non-aqueous-phase liquid (NAPL) occurs as a result of surface spills, tank leaks, and improper disposal practices. Once introduced to the soil, NAPL will migrate downward through the unsaturated zone. In an unconfined aquifer, NAPL less dense than water (LNAPL) will pool above the water-saturated pores of the capillary fringe as an immiscible fluid. As it continues to collect, the NAPL will also move laterally, slightly displacing the capillary fringe due to changes in capillary and gravitational forces.

NAPL components and chemicals will partition into the aqueous and air phases present in the aquifer. As a result, NAPL dissolution into the ground water can contaminate an aquifer for decades (Hunt et al. 1988). The development of the technology for dealing with NAPL lags behind the technology developed for many other ground-water contamination problems. The effective and economical design of a remediation system is dependent on predicting the position and the geometry of the NAPL.

Beginning in the late 1960s, numerous column and two-dimensional (2D) experimental investigations were conducted that improved the physical understanding of the flow of LNAPL and dense NAPL (DNAPL) (e.g., Schwille 1967, 1984, 1988; Eckberg and Sunada 1984; Schiegg and McBride 1987; Carey et al. 1989; Abdul 1988). Two-dimensional experiments were conducted that included the evaluation of surfactant enhanced remediation ("Underground" 1979; Chevalier et al. 1996). Kueper et al. (1989) conducted 2D experiments that evaluated NAPL flow through a model with well-defined lenses of heterogeneity. Experiments of this nature elucidate flow dynamics, but are difficult to utilize as tools for numerical model verification without additional, and often intensive, data. Without verification, numerical models are of limited use. More recently, physical laboratory apparatuses have been equipped to provide simultaneous measurement of quantitative data. The instruments used include dual-gamma attenuation systems (Høst-Madsen and Høgh Jensen 1992) or concurrent electrical resistance and tensiometer readings (Pantazidou and Sitar 1993). In systems of this nature, fluid saturations and pressure measurements are collected to provide empirical coefficients for equations describing the constitutive relationships between pressure, saturation, and permeability. This allows for model verification within the particular system studied.

In site investigation, there is a need to initially identify the geometry and location of a NAPL lens at a site prior to the integration of multiphase models that require an intensive database to predict the flow and transport of NAPL. In response, models have been developed to predict the thickness of an LNAPL lens based on the thickness of NAPL in an observation well, soil properties, and the fluid and capillary characteristics of the fluids (Schiegg 1984; Testa and Packowski 1989; Farr et al. 1990; Lenhard and Parker 1990). Pantazidous and Sitar (1993) and Schroth et al. (1995) present similar equations for estimating the thickness of the lens independent of the NAPL thickness in a monitoring well.

The overall objective of this research was to perform an experimental and numerical investigation of the thickness of a gasoline lens in an unconfined aquifer, and subsequent capillary pollution. To meet this objective, experiments were conducted in a large 2D experimental apparatus that reproduced the capillary, gravitational, and viscous forces that act in the field. In the experiments, gasoline was released into silica sand. A numerical model is developed to predict the thickness of the lens based on the displacement pressure in the lateral direction. The model is compared with the models that predict the lens thickness independent of fluid levels in a monitoring well (Pantazidous and Sitar 1993; Schroth et al. 1995) using the experimental data and additional published data. In addition, the concept of a modified capillary fringe due to capillary pollution is investigated.

## BACKGROUND

Above the phreatic surface in an unconfined aquifer, a region of the soil, called the capillary fringe, is saturated with water under negative pressure. Assuming that the density of air, $\rho_a$, is negligible, the height of the capillary fringe, $h_{cf}$, may be estimated as

$$h_{cf} = \frac{p_c}{\rho_w g} = \frac{4\sigma_{aw}}{d\rho_w g} \tag{1}$$

where $p_c$ = capillary pressure; $\rho_w$ = density of water, $g$ = constant of gravitational acceleration; $\sigma_{aw}$ = air-water interfacial tension; and $d$ = characteristic pore dimension. This equation is derived from the Laplace equation for capillarity

$$p_c = p_{aw} - p_w = (\rho_w - \rho_{aw})gh_c = \frac{4\sigma_{aw}\cos\theta_w}{d} \tag{2}$$

where $d$ = diameter of a capillary tube; $h_c$ = capillary height

---

[1]Asst. Prof., Dept. of Civ. Engrg., Southern Illinois Univ. at Carbondale, Carbondale, IL 62901-6603.

Note. Editor: Byung R. Kim. Discussion open until July 1, 1998. To extend the closing date one month, a written request must be filed with the ASCE Manager of Journals. The manuscript for this paper was submitted for review and possible publication on February 10, 1997. This paper is part of the *Journal of Environmental Engineering*, Vol. 124, No. 2, February, 1998. ©ASCE, ISSN 0733-9372/98/0002-0156-0161/ $4.00 + $.50 per page. Paper No. 15129.

in the tube; and the subscripts nw and $w$ refer to the nonwetting and wetting fluids, respectively. These terms wetting and nonwetting indicate a fluid's preference to adhere to the soil. In the hydrophilic soils investigated, water is the wetting fluid with respect to the nonwetting fluids air or NAPL, and NAPL is the wetting fluid with respect to the nonwetting fluid air. When all three phases occupy a pore space, NAPL becomes an intermediate fluid with respect to the wetting fluid water and the nonwetting fluid air.

Fig. 1 illustrates a generalized capillary height versus saturation curve. Variations in the size and distribution of the soil pores will influence the shape of this curve. This generalized schematic illustrates how soils that exhibit a uniform pore size distribution, such as uniform sand, have a relatively flat slope between the residual saturation of water, $S_{rw}$, and $h_{cf}^{min}$. In contrast, a soil with a large pore-size distribution exhibits a greater curvature in this region. Focusing on the soil with a uniform pore-size distribution, an estimate for the height of the capillary fringe, $h_{cf}$, is shown at the air entry pressure, $h_{cf}^{min}$. A second estimate, $d_{cf}^{avg}$, is shown approximately midway between $S_{rw}$ and $h_{cf}^{min}$. The air entry pressure, which is defined as the pressure needed to displace water in tension-saturated soil, is equivalent to $h_{cf}^{min}$.

Noting that an oil film of only molecular thickness irreversibly transforms a water-air meniscus into a double meniscus composed of a water-oil meniscus and an oil-air meniscus, Schiegg (1984) introduced the concept of a polluted capillary fringe. At a macroscopic view, the double meniscus can be replaced by a fictitious water-air meniscus called a polluted meniscus. Hence, a clear distinction can be made between the capillary fringe region prior to and after the flow of NAPL into the subsurface. Schiegg further defines the polluted capillary pressure, $p_c^{poll}$, and subsequent polluted capillary height, $h_{cf}^{poll}$, as

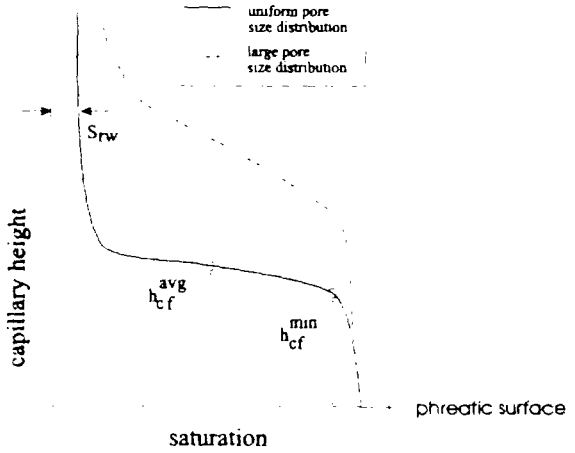


**FIG. 1. Generalized Schematic of Capillary Height versus Saturation Curve Adapted from Schiegg (1984) and Corey (1986)**

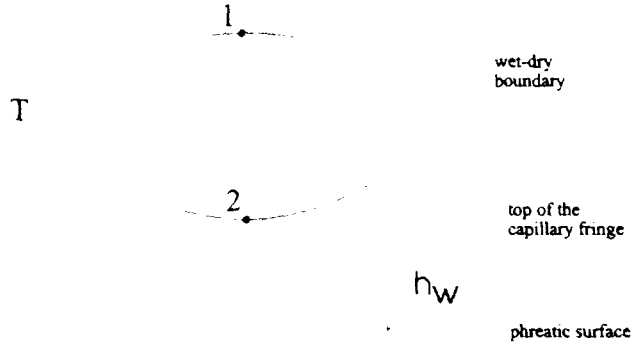


**FIG. 2. Schematic of LNAPL Lens as Presented by Pantazidou and Sitar (1993)**

$$p_c^{poll} = p_c^{ao} + p_c^{ow} \tag{3}$$

$$h_{cf}^{poll} = \frac{p_c^{ao} + p_c^{ow}}{\rho_w g} = \frac{4(\sigma_{ao} + \sigma_{ow})}{\rho_w g d} = h_c^{ao}\rho_o + h_c^{ow}(1 - \rho_o) \tag{4}$$

where $\sigma_{ow}$ = NAPL-water interfacial tension ("o" stands for "oil" and is commonly-used literature to refer to NAPL); and $\rho_o$ = NAPL density. Recognizing the difference between the conventional definition of the capillary fringe and the concept of a polluted capillary fringe, this paper will refer to the region saturated with water above the phreatic surface as the tension-saturated region.

Pantazidou and Sitar (1993) conducted experiments using crystal silica sand and kerosene. To compute the thickness of the lens, an equation was developed for the balance of forces acting at two points at the centerline of the upper and lower boundaries (Fig. 2)

$$T = \frac{1}{\rho_o g}\left[\frac{4(\sigma_{ow} + \sigma_{ao})}{d} - \rho_w g h_w\right] \tag{5}$$

where $T$ = maximum vertical thickness; and $h_w$ = height of point 2 above the phreatic surface.

Schroth et al. (1995) conducted similar experiments in silica sands using soltrol and mineral oil. By estimating the height $h_w$ as

$$h_w = h_{cf} - T \tag{6}$$

(5) is further simplified to

$$T = \frac{4(\sigma_{aw} - \sigma_{ao} - \sigma_{ow})}{dg(\rho_w - \rho_o)} \tag{7}$$

Recognizing that the term $\sigma_{aw} - \sigma_{ao} - \sigma_{ow}$ is the spreading coefficient, this equation is limited to LNAPL ($\rho_w < \rho_o$) with a positive spreading coefficient.

## PHYSICAL MODEL DESCRIPTION, MATERIALS, AND METHODS

A glass tank (1 m × 1 m × 5 cm) was used to maintain a hydrophilic surface (Fig. 3). Of note, the walls of a prototype tank were made of Plexiglas, which has a hydrophobic surface. As a result, a NAPL spill exhibited a distinctly different spreading rate and geometry, indicating that the wall material played a significant role in the flow dynamics. Therefore, the tank was made of glass. Sheets of Plexiglas were placed between the glass face of the model and the additional support

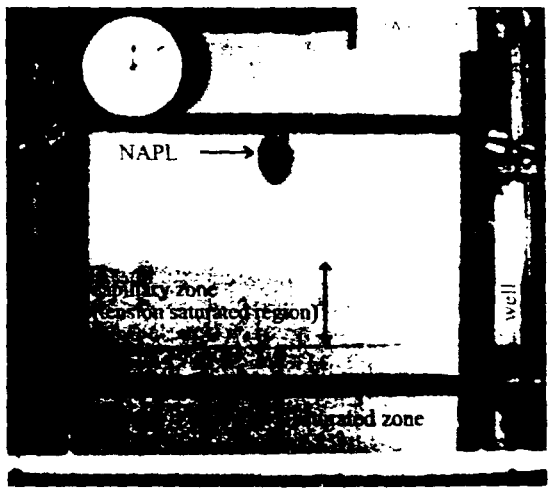


**FIG. 3. Experimental Apparatus after Packing and Establishing Static Capillary Fringe and Vadose Zone. Initial Release of Gas Is Shown by Darker Color in Upper Region of Vadose Zone (Chevalier et al. 1996)**

TABLE 1. Fluid Properties

| Fluid (1) | $\rho$ (g/cm$^3$) (2) | $\sigma_{ow}$ (dyne/cm) (3) | $\sigma_{ao}$ (dyne/cm) (4) | Reference (5) | Spreading coefficient (dyne/cm) (6) |
|---|---|---|---|---|---|
| Gasoline | 0.75 | 12.2 | 20.2 | Farr et al. 1990 | 39.6 |
| Gasoline | 0.75 | 50 | 21 | Mercer and Cohen 1990 | 1 |
| Kerosene | 0.8 | 48 | 27.5 | Pantazidou and Sitar 1993) | −3.5 |
| Soltrol | 0.81 | 41.8 | 25.9 | Schroth et al. 1995 | 4.3 |
| Mineral oil | 0.86 | 38.9 | 30.1 | Schroth et al. 1995 | 3 |

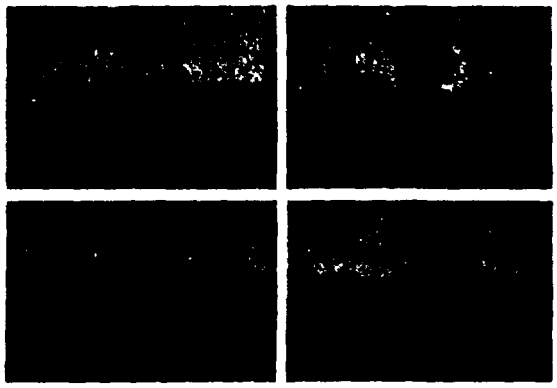

FIG. 4. Sequence of Photographs Showing NAPL Actual Spill (Chevalier et al. 1996)

provided by a steel frame. The tank was designed with wells at the vertical outer edges to establish the location of the water table. External constant head reservoirs were used to control the water level in these wells. The model was wet packed to ensure a homogenous sand matrix. A procedure was established to maintain 5 cm of water above the sand while adding sand to the tank in even lateral sweeps. A medium white 40-mesh Ottawa sand obtained from Soiltest (Lake Bluff, Ill.) was used throughout the experiments presented in this paper. In separately packed column experiments, the porosity measured 0.38 ± 0.01 and the saturated conductivity measured 0.102 ± 0.004 cm/s. It is reasonable to assume that the organic concentration of the sand was low.

After the model was wet packed, the water table was lowered approximately 15 cm every 15 min until a fixed static water table was established 24 cm from the bottom of the tank. The sand was allowed to drain for 24 h, although it appeared to be stable within 1 h. Once the water table was established, the boundary between the saturated and unsaturated zones was easily distinguished, as evident in Fig. 3. The location of the water table was identified by a horizontal line drawn on the outside surface of the front face. An injection well 1 cm in diameter was placed at the centerline 21 cm below the sand surface and within the vadose zone.

Unleaded gasoline and tap water were used at room temperature. Fluid properties are given in Table 1. The gasoline was dyed with an oil red biological stain (Aldrich Chemical Co., Milwaukee, Wis.) to follow fluid movement in the soil matrix. An adsorption isotherm test confirmed that the dye did not sorb to the soil particles. The white sand provided the contrast necessary to distinguish boundaries in black and white photographs.

## EXPERIMENTAL RESULTS

Prior to the release of the gasoline, the Ottawa sand provided a 14.1-cm-thick capillary fringe. A fixed volume (300 ml) of red-dyed gasoline was released from the injection well below the soil surface at an approximate rate of 30 ml/min. Fig. 3 shows the early stage of the spill, as evident by the dark pool in the vadose zone. A sequence of photographs documenting the formation of the gasoline lens is provided in Fig. 4. Although not visually apparent in the black and white photographs, the gasoline left an area of residual oil in the vadose zone. The height of the tension-saturated region of water was reduced to approximately 10.7 cm along the entire width of the model after the NAPL lens was established. Of note, Fig. 4 shows part of a sequence of photographs documenting the mobilization of a LNAPL lens due to surfactants (Chevalier et al. (1996). In the fourth frame of the sequence, a dark color is evident in the upper region of the frame. The dark spot documents the initial release of the surfactant. However, the reduced height of the polluted capillary fringe was established prior to the release of surfactant.

The thickness of the lens in the experiment is determined visually. In Fig. 4, the final lens thickness is estimated as 5.4 cm. However, a small lens of higher saturation was observed immediately above the main lens. This is probably the result of regional heterogeneity, which was only evident from the front face. If this region is included in the reported value for the observed vertical thickness of the lens, the thickness is estimated as 7.5 cm.

In some experimental runs, the gasoline flowed laterally through unseen preferential channels to form secondary pools of gasoline a short distance from the primary lens. However, the overall dimensions of the lens were similar. This shows the sensitivity of the advancing gasoline front to minor variations in the soil matrix. It can be expected that the model is more homogeneous than typical field conditions.

## MODEL DEVELOPMENT

To verify their vertical equilibrium model [see (5)], Pantazidou and Sitar (1993) used an experimentally observed value of $h_w$. However, they state that in the absence of an observed value, the height of the capillary fringe, $h_{cf}$, is a good estimate of $h_w$. Substituting (1) as an expression for $h_w$ in (5), the following equation is obtained:

$$T = \frac{4(\sigma_{ao} + \sigma_{ow} - \sigma_{aw})}{\rho_o d g} \tag{8}$$

If this estimation of $h_w$ is valid, this equation can be used to determine the thickness of the lens when the NAPL-water-air system has a negative spreading coefficient. However, this equation, together with the vertical equilibrium models represented by (5) and (7), neglect the concept of capillary pollution introduced by Schiegg (1984). To support this statement, a simply capillary tube model is used to derive (5).

Fig. 5 shows a capillary tube model with three phases, including an illustration of the forces at each interface. Summing the forces in the vertical direction

$$\pi d\sigma_{ao} + \pi d\sigma_{ow} = \rho_o g h_o \frac{\pi d^2}{4} + \rho_w g h_w \frac{\pi d^2}{4} \tag{9}$$

where $d$ = diameter of the tube and $h_o$ is the height of the oil. Further simplifying this equation

$$4(\sigma_{ao} + \sigma_{ow}) = \rho_o g d h_o + \rho_w g d h_w \tag{10}$$

Solving for $h_o$, this equation is equivalent to (5) in that $h_o$ is equivalent to $T$. It should be noted that $h_w$ in Fig. 5 correlates to $h_w$ in Fig. 2.

If one considers the height of oil as only a thin layer (e.g., $h_o$ is negligible), an expression for $h_w$ can be estimated from

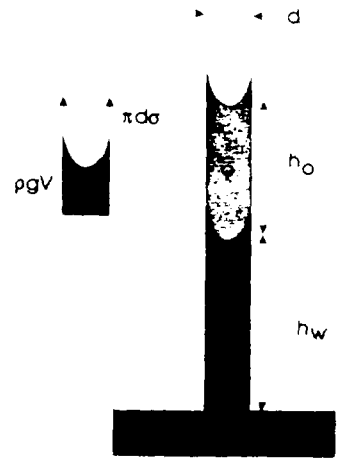


**FIG. 5. Capillary Tube Model with Three Phases Including Illustration of Capillary and Gravitational Forces at Interface**

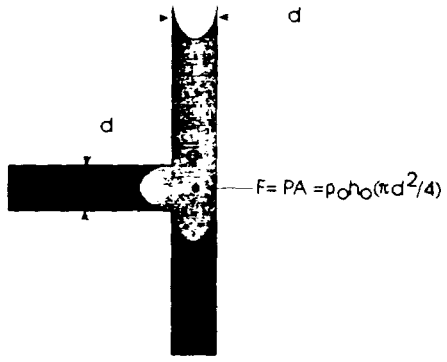


**FIG. 6. Capillary and Pressure Forces in Lateral Branch of Capillary Tube Model**

(10) that is equivalent to the estimate of the polluted capillary fringe height, $h_{cf}^{poll}$ [see (4)]. Further comparing this expression to (1), it can be concluded that the height of the polluted capillary fringe will be different from the original height of the capillary fringe, unless the spreading coefficient is zero (i.e., $\sigma_{ow} = \sigma_{ao} + \sigma_{ow}$). As more oil is introduced into the capillary tube, or the porous media, $h_w$ should decrease as $h_o$ increases.

Unlike the capillary tube, flow in porous media can also occur laterally. Similar to the curved interface in the vertical direction, a curved interface due to capillary forces is also present in the lateral direction within a pore. Recognizing that the hydrostatic pressure due to the height of the oil is greatest within the pore with the interface preventing vertical flow, the capillary tube model will be modified to evaluate the displacement of water in the lateral direction (Fig. 6). The position and curvature of the interfaces are exaggerated to illustrate the concepts. Since the characteristic pore dimensions are equal in all direction, this tube will have the same diameter as the tube in the vertical direction. Summing the forces in the horizontal direction

$$\pi d\sigma_{ow} - h_o\rho_o g\frac{\pi d^2}{4} = 0 \tag{11}$$

Flow in the lateral direction will only occur when the hydrostatic pressure at this interface due to the height $h_o$ exceeds the capillary pressure between the oil and water. This pressure is referred to as the displacement pressure, $p_d$. After the release of oil ceases, the lateral spread will discontinue, establishing an equilibrium thickness of the lens at the value of $h_o$, which created the initial displacement pressure

$$h_o = T = \frac{4\sigma_{ow}}{\rho_o g d} \tag{12}$$

## RESULTS AND DISCUSSION

The choice of two critical parameters should be discussed at this point: (1) The characteristic pore dimension; and (2) the delineation of the outer boundary of the lens. The choice of an appropriate characteristic pore diameter is critical. Since the oil is displacing water (i.e., drainage of the wetting phase), the controlling diameter is the pore neck, as opposed to the pore body. Ng et al. (1978) report that the diameter of a pore throat opening, $d_n$, for a random packing of sphere can be predicted from the average diameter of a sphere

$$d_n = 0.42d_{avg} \tag{13}$$

Pantazidou and Sitar (1993) consider this equation when fitting an equation to their data and estimating $d_n$ as $0.4d_{avg}$. The pore throat opening can also be estimated from the experimentally measured height of the capillary fringe using (1) (Schroth et al. 1995). This definition assumes that the visibly wet-dry boundary observed in the 2D experiments coincides with $h_{cf}$.

It is important to recognize that the equilibrium models for estimating the thickness of the lens are estimating the region where NAPL saturations are high. This estimate is reasonable, since a large percent of the NAPL volume is within this lens, but the actual region contaminated with NAPL is much larger. This is illustrated in part in Fig. 7, which shows generalized capillary height-saturation curves in a three-phase environment. In these curves, as well as in Fig. 1, $h_c$ and $h_{cf}$ are analogous to the displacement head, $p_d/\rho g$. Due to the migration of the oil, a variable residual oil-phase saturation remains in the vadose zone. This residual saturation is low in the upper regions of the spill path, and increases as the depth increases. The top of the lens in the gasoline experiments is identified by a relatively distinct boundary of higher NAPL saturation. Below the lens, NAPL is also found at lower saturations that may be trapped as small isolated and discontinuous droplets, referred to as ganglia. This was also observed in the experiment.

In the experiment, the capillary fringe area is estimated at 14.1 cm. Using (1) and $\sigma_{ow}$ = 72 dyne/cm, the characteristic dimension is calculated as 0.02 cm, which agrees reasonably well with the dimension predicted from a random packing of spheres using $d_{50}$ (0.042 cm) as an estimate of $d_{avg}$, 0.017 cm. The zone of tension saturated water is reduced to 10.7 cm in the regions of the model beyond the lens, illustrating the capillary pollution that occurs from a small film of gasoline. Two reported values of interfacial tension for gasoline are referenced in Table 1. The values reported for $\sigma_{ao}$ are in relative agreement (20.2 and 21 dyne/cm). However, the values re-

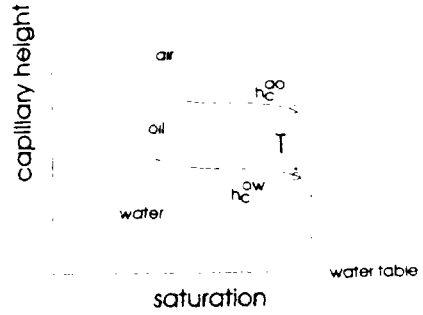


**FIG. 7. Generalized Three-Phase Capillary Height Saturation Curve**

TABLE 2. Comparison of Observed Vertical Thickness of NAPL Lens with Thickness Predicted Using Equilibrium Equations

| NAPL (1) | Soil description (2) | $d$ (cm) (3) | $h_w$ (cm) (4) | $T$ observed (cm) (5) | $T$ Predicted (cm) | | |
|---|---|---|---|---|---|---|---|
| | | | | | Eq. (12) (6) | Eq. (5) (7) | Eq. (7) (8) |
| Gasoline | Ottawa sand | 0.02 | 5 | 5.4/7.5 | 7.9 | 7.5 | 23.8 |
| Kerosene[a] | Fine silica sand | 0.01 | 17.2 | 16.4 | 24.5 | 17.0 | NA[c] |
| Kerosene[a] | Coarse silica sand | 0.02 | 8.4 | 11.3 | 12.2 | 8.7 | NA[c] |
| Soltrol[b] | 12/20 | 0.05 | N/A | 2.75 | 4.2 | N/A | 1.8 |
| Soltrol[b] | 20/30 | 0.03 | N/A | 4.08 | 6.8 | N/A | 3.0 |
| Soltrol[b] | 30/40 | 0.02 | N/A | 4.65 | 10.0 | N/A | 4.4 |
| Soltrol[b] | 40/50 | 0 02 | N/A | 4.92 | 14.0 | N/A | 6.2 |
| Mineral oil[b] | 12/20 | 0.05 | N/A | 3.6 | 3.7 | N/A | 1.7 |
| Mineral oil[b] | 20/30 | 0.03 | N/A | 3.68 | 5.9 | N/A | 2.8 |
| Mineral oil[b] | 30/40 | 0.02 | N/A | 4.62 | 8.8 | N/A | 4.2 |
| Mineral oil[b] | 40/50 | 0.02 | N/A | 4.46 | 12.3 | N/A | 5.8 |

[a]Pantazidou and Sitar (1993); $d$ based on random packing of spheres and reported values of average grain size.
[b]Schroth et al. (1995); $d$ based on random pack of spheres and $d_{50}$ extrapolated from particle size distribution curves. Values of $h_w$ not reported.
[c]Negative spreading coefficient.

ported for $\sigma_{ow}$ are distinctly different (12.2 compared to 50 dyne/cm). Using an average estimate for (20.6 dynes/cm), a reasonable estimate of $\sigma_{ow} = 25.6$ dyne/cm can be made from the experimentally measured $h_{cf}^{pool}$ and (4).

Pantazidou and Sitar (1993) and Schroth et al. (1995) report similar experiments where an LNAPL was released in a model simulating an unconfined aquifer. Their reported data, together with the gasoline experiment, provide a database for evaluating the models reviewed and developed in this paper. The data from their experiments is summarized in Tables 1 and 2.

In Table 2, the observed thickness of a NAPL lens is compared to the thickness predicted using (12) in addition to the vertical equilibrium models developed by Pantazidou and Sitar (1993) [see (5)] and Schroth et al. (1995) [see (7)]. The estimates of $d$ are based on $d_{50}$ and (13). The use of (7) is limited to fluid pairs that exhibit a positive spreading coefficient. Although Schroth et al. (1995) report that (5) accurately predicts the thickness of a lens when compared to their experimental data, they do not report the observed values of $h_w$.

Both Pantazidou and Sitar (1993) and Schroth et al. (1995) report that the height of the tension saturated remained constant after the NAPL lens was formed. As stated previously, (4) illustrates that a spreading coefficient approximately equal to zero will not effect the height of the tension-saturated region. Since the spreading coefficients of kerosene, soltrol, and mineral are near zero, their observations are in agreement with (4).

The models all predict an increase in the lens thickness as $d$ decreases. However, (12) in general, predicts a greater increase. This is particularly evident when comparing (12) and (7) for the experiments involving soltrol and mineral oil. Eq. (7), which assumes that no capillary pollution will occur, matches the observed values more closely. Applying (7) to the gasoline experiment, the greatest difference between the observed and predicted thickness is evident. This is due to the fact that gasoline is the only NAPL evaluated with a high spreading coefficient, and subsequently, the only NAPL that was observed to reduce the tension-saturated region of water. This observation negates the assumption used to justify the substitution of (6) into (5), and the subsequent derivation of (7).

For the kerosene, which exhibits a negative spreading coefficient near zero, (11) predicts a thickness of 1.78 cm (fine sand) and 0.89 cm (coarse sand). This large error may be explained by the assumption used in developing (11). Pantazidou and Sitar (1993) state that $h_w$ may be predicted from the height of the capillary fringe. In addition, they define the height of the capillary fringe below the visibly wet-dry boundary. As a result, the visibly wet-dry boundary and the top of the capillary fringe are somewhat synonymous to Schiegg's (1984) definitions of the average and minimum $h_{cf}$ (Fig. 1). By substituting $h_{cf}$ for $h_w$, it is assumed that the oil only displaces water in the region above the capillary fringe. However, (10) documents that the thickness of the oil lens reduces $h_w$, which translates into displacing water in capillary fringe. In contrast, Schroth et al. (1995) defines the wet-dry boundary as the height of the capillary fringe. In this definition, there is no attempt to specifically distinguish between the average and minimum $h_{cf}$. Of note, this difference is minimized in uniform sands.

## SUMMARY

To simulate a NAPL spill in an unconfined aquifer, gasoline was released in the vadose zone of a 2D model packed with Ottawa sand. The gasoline also formed a lens above the region of water-saturated pores. A thin film of gasoline migrated beyond the boundaries of the lens to pollute and reduce the height of the capillary fringe. Experimental results were combined with results from similar experiments conducted by other researchers using different sand and NAPL pairs. The general behavior and geometry of the NAPL spills exhibited the same general results. This provided a database for evaluating the equations for predicting the thickness of the lens based on soil and fluid properties. The previously published models reasonably predicted the thickness of the lens when the underlying assumptions regarding the height of the capillary fringe, $h_{cf}$, and the distance between the bottom of the lens and the phreatic surface, $h_w$, were accurate. An additional model for determining the thickness of the lens was derived from the same fluid and soil properties used in the previous models, but also incorporating capillary pressure in the lateral direction. This model is independent of the $h_{cf}$ and $h_w$, avoiding the pitfalls of defining these parameters. The model performed reasonably well. All of the models evaluated assume that the thickness of the lens is reasonably estimated over a region of high NAPL saturation, where the largest volume of the NAPL is encountered.

## ACKNOWLEDGMENTS

The writer is grateful to Dr. Roger B. Wallace and Dr. David C. Wiggert, Department of Civil and Environmental Engineering at Michigan State University, for support in the experimental portion of this research. The writer would also like to thank the anonymous reviewers for providing valuable comments.

## APPENDIX I. REFERENCES

Abdul, A. S. (1988). "Migration of petroleum products through sandy hydrogeological systems." *Ground Water Monitoring and Remediation*, 8, 73–81.

Carey, J. W., Simmons, C. S., and McBride, J. F. (1989). "Predicting oil infiltration and redistribution in unsaturated soils." *Soil. Sci. Soc. Am. J.*, 53, 335–342.
Chevalier, L. R., Wallace, R. B., Wiggert, D. C., and Shabana, M. D. (1996). "2-D experimental investigation of surfactant mobilization of light nonaqueous phase liquid." *Non-aqueous phase liquids in the subsurface environment: assessment and remediation*, L. N. Reddi, ed., ASCE, Washington, D.C., 3517–368.
Corey, A. T. (1986). "Mechanics of immiscible fluids in porous media." *Water Res.*
Eckberg, D. K., and Sunada, D. K. (1984). "Nonsteady three-phase immiscible fluid distribution in porous media." *Water Resour. Res.*, 20, 1891–1897.
Farr, A. M., Houghtalen, R. J., and McWhorter, D. B. (1990). "Volume estimation of light nonaqueous phase liquids in porous media." *Ground Water*, 28(1), 48–56.
Høst-Madsen, O., and Høgh Jensen, K. (1992). "Laboratory and numerical investigations of immiscible multiphase flow in soil." *J. Hydro.*, 134, 13–52.
Hunt, J. R., Sitar, N., and Udell, K. S. (1988). "Nonaqueous phase liquid transport and cleanup: 1. analysis of mechanisms." *Water Resour. Res.*, 24(8), 1247–1258.
Kueper, B. H., Abbott, W., and Farquar, G. (1989). "Experimental observations of multiphase flow in heterogeneous porous media." *J. Contam. Hydro.*, 5, 83–95.
Lenhard, R. J., and Parker, J. C. (1990). "Estimation of free hydrocarbon volume from fluid levels in monitoring wells." *Ground Water*, 28(1), 57–67.
Mercer, J. W., and Cohen, R. M. (1990). "A review of immiscible fluids in the subsurface: properties, models, characterization and remediation." *J. Contam. Hydro.*, 6, 107–163.
Ng, K. M., Davis, H. T., and Scriven, L. E. (1978). "Visualization of blob mechanics in flow through porous media." *Chemical Engrg. Sci.*, 33, 1009–1017.
Pantazidou, M., and Sitar, N. (1993). "Emplacement of nonaqueous liquids in the vadose zone." *Water Resour. Res.*, 29(3), 704–722.
Schiegg, H. O. (1984). "Considerations on water, oil and air in porous media." *Water Sci. and Technol.*, 17, 467–476.
Schiegg, H. O., and McBride, J. F. (1987). "Laboratory setup to study two-dimensional multiphase flow in porous media." *Petr. Hydrocarbons and Organic Chemicals in Ground Water Conf.*, Houston, Tex.
Schroth, M. H., Istok, J. D., Ahearn, S. J., and Selker, J. S. (1995). "Geometry and position of light nonaqueous-phase liquid lenses in water-wetted porous media." *J. Contam. Hydro.*, 19, 269–287.
Schwille, F. (1967). "Petroleum contamination of the subsoil-A Hydrological Problem." *Joint problems of oil and water industries*, P. Hepple, ed., Inst. of Petroleum, London, 23–54.
Schwille, F. (1984). "Migration of organic fluids immiscible with Water in the unsaturated zone." *Pollutants in porous media*, B. Yaron, G. Dagan, and J. Goldschmid, eds., Springer-Verlag New York, Inc., New York, 27–48.
Schwille, F. (1988). *Dense chlorinated solvents in porous and fractured media-model experiments*, Translated by J. F. Pankow, Lewis Publishers, Chelsea, Mich., 146.
Testa, S. M., and Paczkowski, M. T. (1989). "Volume determination and recoverability of free hydrocarbon." *Ground Water Monitoring and Remediation*, Winter, 120–128.
"Underground movement of gasoline on groundwater and enhanced recovery by surfactants." (1979). Am. Petr. Inst., *API Publ. No. 4317*.

## APPENDIX II. NOTATION

*The following symbols are used in this paper:*

$d$ = diameter;
$g$ = constant of gravitational acceleration;
$h$ = height;
$h_c$ = capillary pressure head;
$p_c$ = capillary pressure;
$S_{rw}$ = saturation of residual water;
$T$ = vertical lens thickness;
$\rho$ = density; and
$\sigma$ = interfacial tension.

### Subscripts/Superscripts

$a$ = air;
avg = average;
cf = capillary fringe;
min = minimum;
nw = nonwetting fluid;
$o$ = oil;
poll = polluted; and
$w$ = water or wetting fluid.